

S. Richtsmeier and R. Sundberg, Recent advances in the simulation of partly cloudy scenes, Proc. SPIE 7827, Remote Sensing of Clouds and the Atmosphere XV, 78270S (October 11, 2010).

Copyright 2010 Society of Photo-Optical Instrumentation Engineers. One print or electronic copy may be made for personal use only. Systematic reproduction and distribution, duplication of any material in this paper for a fee or for commercial purposes, or modification of the content of the paper are prohibited.

<http://dx.doi.org/10.1117/12.871345>

See next page.

# Recent Advances in the Simulation of Partly Cloud Scenes

Steven Richtsmeier\* and Robert Sundberg  
Spectral Sciences, Inc., 4 Fourth Avenue, Burlington, MA 01803-3304

## ABSTRACT

This paper discusses recent advances in the simulation of spectral scenes with partial cloud cover. We examine the effect of broken cloud fields on the solar illumination reaching the ground. Application of aerosol retrieval techniques in the vicinity of broken clouds leads to significant over-prediction of aerosol optical depth because of the enhancement of visible illumination due to scattering of photons from clouds into clear patches. These illumination enhancement effects are simulated for a variety of broken cloud fields using the MCScene code, a high fidelity model for full optical spectrum (UV through LWIR) spectral image simulation. MCScene provides an accurate, robust, and efficient means to generate spectral scenes for algorithm validation. MCScene utilizes a Direct Simulation Monte Carlo approach for modeling 3D atmospheric radiative transfer (RT), including full treatment of molecular absorption and Rayleigh scattering, aerosol absorption and scattering, and multiple scattering and adjacency effects, as well as scattering from spatially inhomogeneous surfaces.

**Keywords:** Spectral, simulation, scene, algorithm, sensor, visible, infrared

## 1. INTRODUCTION

The effects of broken cloud fields on aerosol retrieval is an active area of research.<sup>1-4</sup> Application of aerosol retrieval techniques in the vicinity of broken clouds, even as far as several kilometers away, leads to significant over prediction of aerosol optical depth because of the enhancement of visible illumination from the scattering of photons from the clouds into clear patches. Several recent papers have examined the impact of 3D clouds on reflectance and aerosol optical depth retrieval.<sup>1-4</sup> This paper presents detailed simulations of the enhanced solar illumination reaching the ground due to scattering from nearby cloud fields. The consequence of this enhanced illumination on aerosol retrieval will be presented in a future publication.

In this paper, we investigate the effect of broken cloud fields on solar illumination reaching the ground. The simulations presented here use a first-principles, high-fidelity spectral image simulation capability, dubbed MCScene, that is based on a Direct Simulation Monte Carlo (DSMC) approach for modeling the 3D radiative transport. The basic methodology used in MCScene has been described previously.<sup>5-7</sup>

## 2. EFFECT OF FINITE 3D CLOUDS

To examine the illumination variations caused by clouds, a highly controlled scene was constructed with a single spherical cloud with diameter 1 km, a base altitude of 0.5 km, and a vertical optical depth of 20, above flat terrain with a uniform reflectance of 0.1. The atmosphere for the simulation was MODTRAN<sup>®</sup>'s<sup>8-9</sup> mid-latitude summer model with rural aerosols and a visibility of 23 km. The left side of Figure 1 shows the scene for a nadir viewing sensor, band pass  $1600\pm 5$  nm, at 20 km altitude. The image measures 9.6 km by 9.6 km. The sun comes from the bottom of the scene at a zenith angle of  $75^\circ$ , and the cloud, located in the center of the scene, casts an elongated shadow behind itself. The sunlit side of cloud, as would be expected, appears brighter than the back side of the cloud, though the back side is still brighter than the ground. At the right of Figure 1, the data is presented as percent enhancement, defined as the percent difference in intensity between each pixel in the cloud scene and an equivalent but cloudless scenario. Clearly apparent in red are pixels indicating enhanced illumination, 20-30% greater than if there was no cloud, due to scattering of photons from the cloud to the ground. The shadow has a depth of about 80%. Also apparent is the path the shadow takes between the cloud and the ground where aerosols are not illuminated.

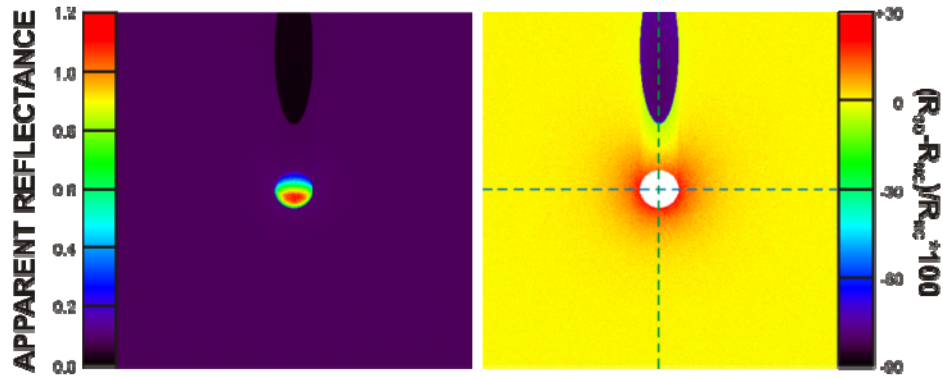


Figure 1. At left, MCScene single band ( $1600\pm 5$  nm) simulation result for a synthetic spherical cloud over flat terrain with a uniform reflectance of 0.1. The image at right provides a relative comparison of the cloud scene simulation with the equivalent cloudless simulation, with cloud pixels masked as white. The dashed lines on the right mark the paths of the cross-sections of Figure 2.

Cross-sections from the right side of Figure 1 are displayed in Figure 2. At the left of Figure 2, the x-axis cross section shows that the enhancement has a maximum of greater than 20% in the vicinity of the cloud, decreasing with increasing distance, until it disappears into the baseline at 2.5 km from the cloud edge. The y-axis cross-section at the right of Figure 2 shows roughly the same distance dependence on the sunlit side of the cloud (positive y-offset), but the enhancement is noticeably suppressed on the back side of the cloud as the cloud shadow propagates through the atmosphere.

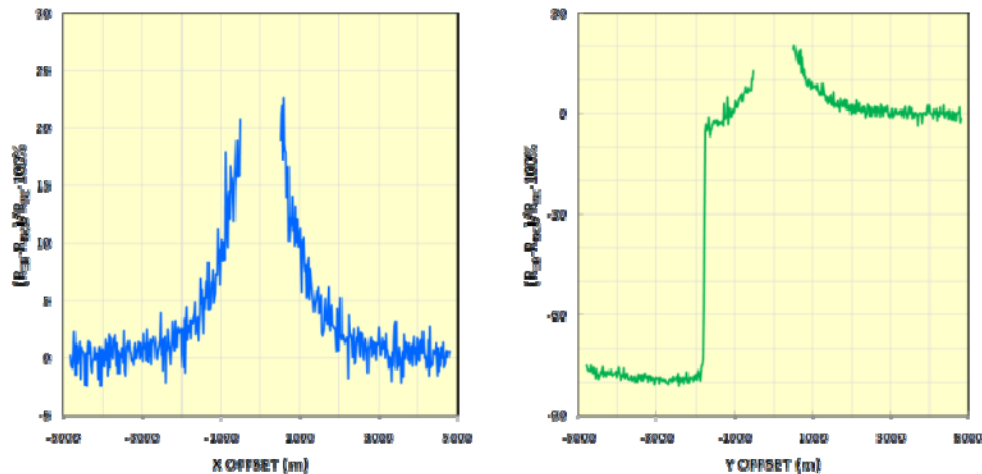


Figure 2. Percent enhancement of top-of-the-atmosphere apparent reflectance for slices across the center of the spherical cloud scene shown in Figure 1.

While Figure 1 depicts a simple scattering scenario, complicated cloud fields yield more complicated secondary illumination effects. Simulations with realistic cloud fields and the resulting enhancement results are shown in Figures 3-8. Three synthetic cloud fields for the simulations were generated by the Cloud Scene Simulation Model (CSSM).<sup>10</sup> CSSM generates high fidelity cloud liquid water content fields in four dimensions based on fractal techniques and using meteorological inputs. The spatially varying optical depths (OD) of the cloud fields generated for this study are shown in Figure 3. The nimbostratus field has a maximum optical depth of 24, while the altostratus and stratocumulus street fields have OD maxima of 9 and 21, respectively. Figure 4 shows a series of images simulated using the three cloud types over flat terrain with a spectrally uniform reflectance of 0.10. For all cases, the sensor was nadir-viewing from 20 km altitude. The MODTRAN<sup>®</sup> atmosphere for these simulations was the mid-latitude summer model with rural aerosols and 23 km ground visibility. Local time for the simulation of Figure 4A was solar noon (i.e., sun from due south) with a solar zenith angle of 17.4°. For the altostratus scene in Figure 4B, local time was solar noon minus 2 hours with a solar zenith angle of 30.5°. Local time for Figure 4C was solar noon plus 2 hours with a solar zenith angle of 30.5°.

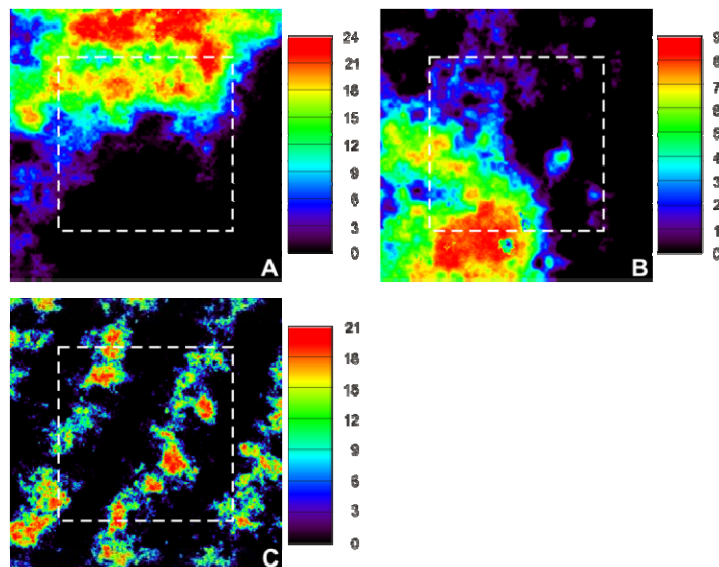


Figure 3. Vertical optical depth maps for three types of cloud fields: (A) nimbostratus, (B) altostratus, and (C) stratocumulus street. The cloud fields measure 15 km on a side. The dashed squares indicate the fields-of-view for the simulations.

The percent change in scene apparent reflectance at 660 nm when compared to the cloud free scene is shown in Figure 5 for each of the three cloud fields. The three scenes represent different scattering scenarios. In Figure 5A, a high south sun shines on a thick nimbostratus field, and photons are backscattered off the clouds onto the open ground to the south. There is little shadowing apparent as the shadows fall underneath the cloud field. Almost all open areas in the scene exhibit enhanced brightness ranging from about 30% near the clouds down to 5% at the bottom edge of the scene, several km away from the cloud field (see Figure 6). There are also areas visible through holes in the clouds where the enhancement runs from 30% to as high as 64%. Here, the holes or convoluted cloud field edges serve as conduits for photons.

In Figure 5B, the sun comes from the south west at 30.5° over the top of a moderately dense altostratus field. There are shadows of varying depth due to the spatially varying density of the cloud field. There is significant enhancement apparent in unshaded areas, ranging from about 15% near shadow edges down to about 3% at the furthest distance from the clouds. Whereas the enhancement in the nimbostratus scene was due to backscattering, the enhancement in Figure 5B is due predominately to forward scattering of photons off of or through the cloud tops.

Figure 5C effectively represents a mix of the scenarios of 5A and 5B, as a 30.5° sun shines from the south west, perpendicular to the roughly parallel rows of a stratocumulus street field. Here, backscattering from the eastern face of a cloud row is met by the forward scattering and shadows from its eastern neighbor row. As a result, enhancement is noticeably greater in unshaded areas than for either of the nimbostratus or altostratus scenarios. As was the case for the nimbostratus scene, convoluted cloud edges facing the sun result in greater enhancement near the clouds. The shadows in the stratocumulus scene are more dense than the altostratus shadows (as the clouds are more dense), but the edges of these shadows are softened by the backwash of photons from a neighboring row of clouds.

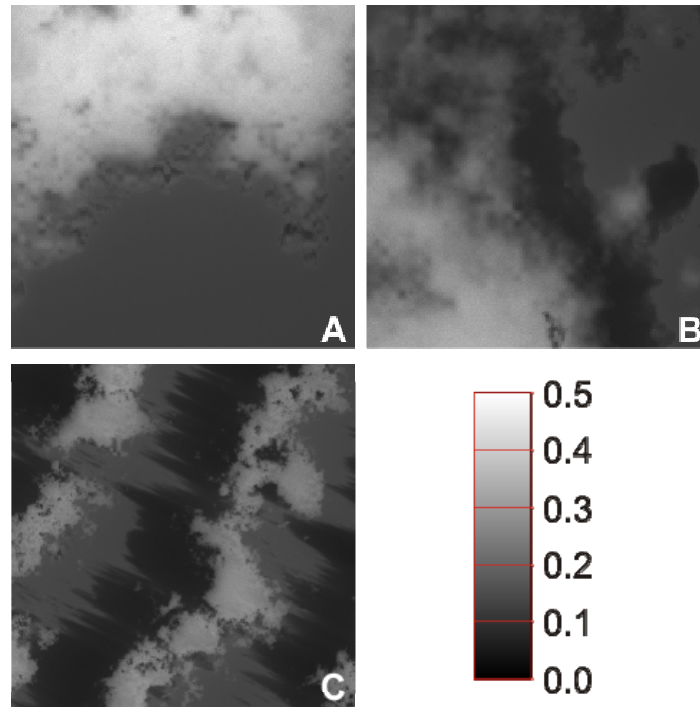


Figure 4. Apparent reflectance for a sensor band of  $660\pm 5$  nm for scenes containing three types of cloud fields: (A) nimbostratus, (B) altostratus, (C) stratocumulus street, over flat terrain with uniform reflectance of 0.10. Sensor fields-of-view are 10 km x 10 km.

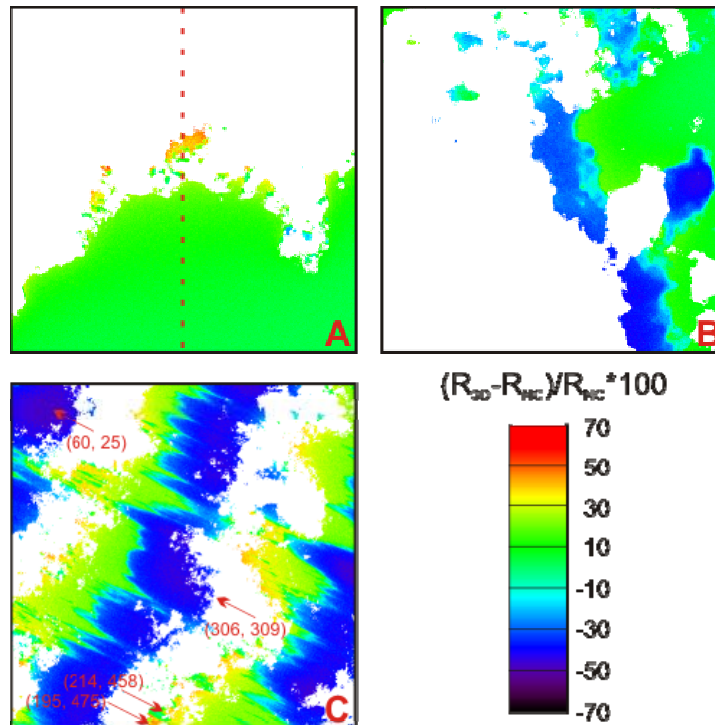


Figure 5. Percent enhancement to apparent reflectance for  $660\pm 5$  nm for scenes with three synthetic cloud fields: (A) nimbostratus, (B) altostratus, and (C) stratocumulus street. Pixels containing cloud are masked white. The red dashed line in "A" marks the path of the enhancement profile of Figure 6. Reflectance spectra for labeled pixels in C are plotted in Figure 7.

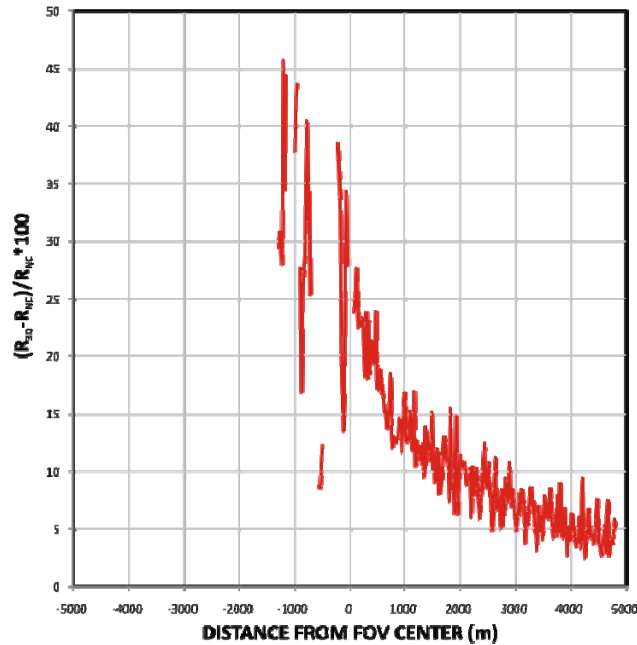


Figure 6. Y profile of 660 nm enhancement through the center (dashed line) of the nimbostratus scene of Figure 5A.

Reflectance spectra for several pixels labeled in Figure 5C are shown in Figure 7. These include a cloud top pixel, a pixel in deep shadow, one exhibiting near-maximum enhancement for this scene, and one that mixes enhancement and shadow. Also shown for reference is a cloud-free spectrum and the uniform source reflectance for the ground. There is a spectral dependence to the enhancement effect. Comparing the “enhanced” and “no cloud” pixels, enhancement is greater in the infrared than the visible, approaching a factor of two from 800 to 1800 nm. Comparing the “shadow” and “no cloud” curves, shadows are deeper in the infrared, presumably because they are not back-filled by Rayleigh scattering as they are in the visible. Curiously, comparing the mixed “enhanced + shadow” curve with the “no cloud” curve shows that they are nearly identical from about 1100 nm to longer wavelengths.

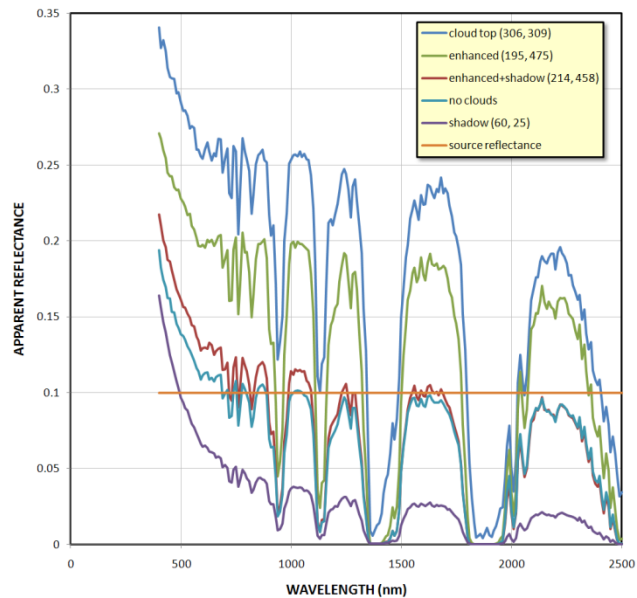


Figure 7. Comparison of pixel spectra for several points from Figure 5C, along with the spectrum from a cloudless scene, and a line marking source reflectance of the ground.

Figure 8 demonstrates how the intensity of secondary illuminations is coupled to the geometry, specifically, the interaction of 3D cloud structure and solar position. Plotted are simulations of the stratocumulus street cloud scene for three solar positions. In Fig 8A, local time was solar noon minus 2 hours with a solar zenith angle of 30.5°. Here, the solar direction is roughly perpendicular to the direction of the cloud “streets”. (This is the same plot as Figure 5C.) The combination of back scattering from eastern cloud faces with forward scattering from the top of the neighboring street to the west results in typical illumination enhancement in unshaded areas of 20-40%, in some places < 50% near convoluted cloud edges. Local time for the simulation of Figure 8B was solar noon with a solar zenith angle of 17.4°. The sun is higher in the sky, so shadows are more confined to lie beneath the clouds. However, compared to Figure 8A, illumination enhancement in unshaded areas is typically only 17-25%, with only a handful of pixels reaching 40%. For Figure 8C, local time was solar noon plus 2 hours with a solar zenith angle of 30.5°. Illumination enhancement here is 20-30% in non-shaded areas, greater than the solar noon case, but less than the geometrically optimal case of solar noon minus two hours.

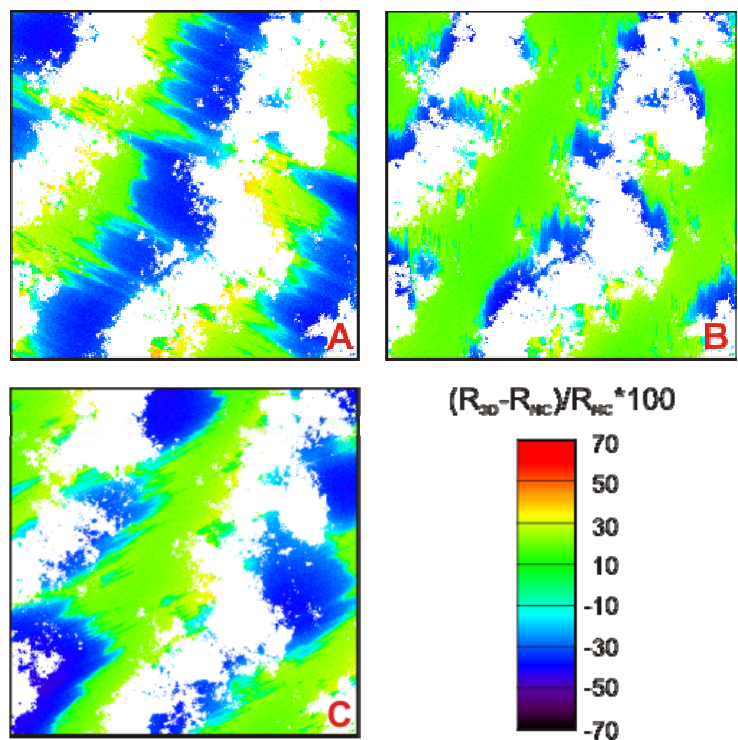


Figure 8. Percent enhancement to simulated apparent reflectance at 660±5 nm for the stratocumulus street cloud field for three solar positions: (A) solar noon minus two hours, (B) solar noon, and (C) solar noon plus two hours. Pixels containing cloud are masked white.

We have recently been working on adding look-up capability to MCSce. Some preliminary results are presented in Figure 9. For these simulations, the observer is placed on the ground and looks up with a full hemispherical view of the sky. At left, the observer sees the altostratus cloud field of Figure 4 with the local time set to solar noon plus two hours. At right, the observer sees the stratocumulus street field with the local time set to solar noon minus two hours. In both cases, the observer stands in shadow at the centers of the respective scenes of Figure 4. In the altostratus image, the cloud bottom appears brightest where the solar position is roughly aligned with a thin spot in the clouds (position “1”). In the stratocumulus image, where the sun comes from the lower right, the brightest illumination comes from where the photons skim the top of the eastern “street”. Representative spectra from the positions marked in the altostratus scene are shown in Figure 10.

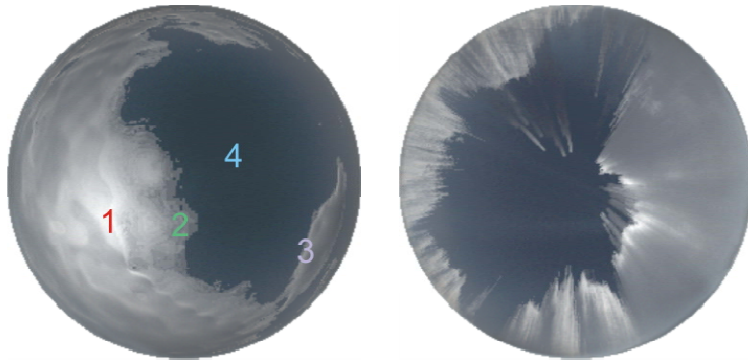


Figure 9. RGB composite hemispherical images, from the ground looking up, from the centers of the altostratus (left) and stratocumulus street (right) scenarios of Figure 4.

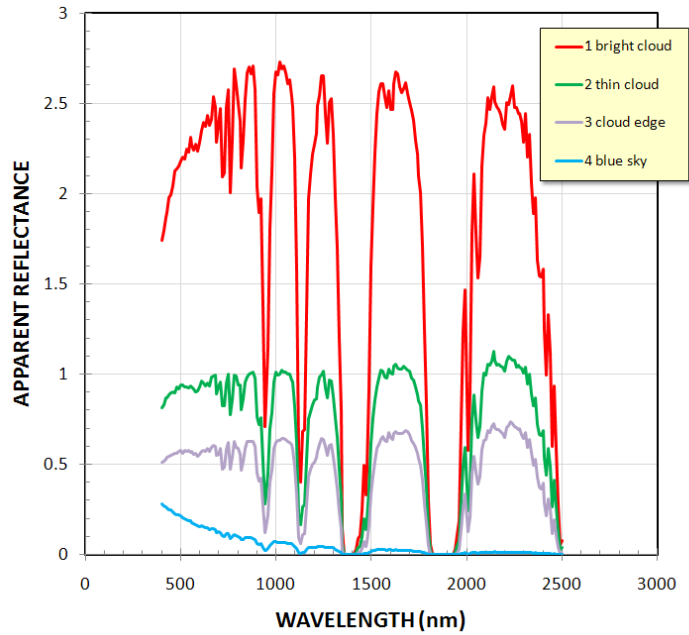


Figure 10. Representative spectra from the look-up image for the altostratus scene of Figure 9.

### 3. CONCLUSIONS

A practical, first-principles simulation model for spectral imagery, based on a Direct Simulation Monte Carlo (DSMC) radiative transport approach, has been used to investigate the enhanced radiation in sunlit areas caused by scattering of photons from broken cloud fields. The enhancement shows spectral and spatial dependence and is present in both forward and back scattering scenarios. The effect diminishes as distance from the cloud increases. Key parameters to developing a model for the effect include cloud type and density, and the coupling of solar position with cloud spatial geometry.

The effects of broken cloud fields on aerosol retrieval will be examined in a future paper. Application of aerosol retrieval techniques in the vicinity of broken clouds leads to significant over prediction of aerosol optical depth because of the enhancement of visible illumination from the scattering of photons from the clouds into the clear patches. Simulations such as shown in this paper should aid in the development of a technique to produce accurate aerosol optical depths near broken clouds.

#### 4. ACKNOWLEDGMENT

The authors wish to acknowledge Spectral Sciences, Inc. for support under an internal research and development grant, and the Air Force Research Laboratory, RVBYM for support under contract number FA8718-07-C-0048.

#### REFERENCES

- [1] Wen, G., Marshak, A., Cahalan, R., "Impact of 3D clouds on clear sky reflectance and aerosol retrieval in a biomass burning region of Brazil," *J. Geophys. Res.* 112:D13204 (2006).
- [2] Marshak, A., Wen, Coakley, G., J., Remer, L., Loeb, N., Cahalan, R., "A simple model for the cloud adjacency effect and the apparent bluing of aerosols near clouds," *J. Geophys. Res.* 113:D14S17 (2008).
- [3] Kassianov, E., Ovtchinnikov, M., "On reflectance ratios and aerosol optical depth retrieval in the presence of cumulus clouds," *Geophys. Res. Lett.* 35: L06807 (2008).
- [4] Kassianov, E., Ovtchinnikov, M., Berg, L., McFarlane, S., and Flynn, C., "Retrieval of aerosol optical depth in vicinity of broken clouds from reflectance ratios: Sensitivity study," *JQSRT* doi:10.1016/j.jqsrt.2009.01.014 (2009).
- [5] Richtsmeier, S.C., Berk, A., Adler-Golden, S.M., and Bernstein, L.S., "A 3D Radiative-Transfer Hyperspectral Image Simulator for Algorithm Validation," *Proceedings of ISSSR 2001*, Quebec City, Canada (June 2001).
- [6] Sundberg, R.L., Kennett, R., Richtsmeier, S.C., Gruninger, J., Berk, A., and Matthew, M., "Hyperspectral Scene Simulation in the Ultraviolet through Longwave Infrared," Phase II Final Report, prepared for AFRL, Sensors Directorate WPAFB, under Contract No. F33615-02-C-1167 (2005).
- [7] Richtsmeier, S., Sundberg, R., and Clark, F.O., "Fast Monte Carlo Full Spectrum Scene Simulation," *Proceedings of the International Radiation Symposium 2008*, Foz do Iguacu, Brazil (August 2008).
- [8] Berk, A., Bernstein, L.S., and Robertson, D.C., "MODTRAN<sup>®</sup>: A Moderate Resolution Model for LOWTRAN 7," GL-TR-89-0122, Geophysics Directorate, Phillips Laboratory, Hanscom AFB, MA 01731 ADA214337 (April 1989).
- [9] Berk, A., et. al., "MODTRAN<sup>®</sup>5: 2006 update," In *Algorithms for Multispectral, Hyperspectral, and Ultraspectral Imagery XII*, Sylvia S. Chen, Paul E. Lewis, Editors, *Proceedings of SPIE Vol. 6233*, (2006).
- [10] Cianciolo, M.E., and Raffenberger, M.E., "Atmospheric Scene Simulation Modeling and Visualization (AMV)," *Cloud Scene Simulation Model User's Guide*, TIM-07169-2, TASC, Reading, MA, (1996).